Meas. Sci. Technol. **22** (2011) 035206 (13pp) doi:10.1088/0957-0233/22/3/035206

Influence of the gauge length on the accuracy of long-gauge sensors employed in monitoring of prismatic beams

Branko Glisic

Princeton University, E330, EQuad, Princeton, NJ 08544, USA

E-mail: bglisic@princeton.edu

Received 14 July 2010, in final form 22 December 2010
Published 15 February 2011
Online at stacks.iop.org/MST/22/035206

Abstract

Depending on the geometric basis of measurement (gauge length), discrete strain sensors used in structural monitoring of civil engineering structures can be considered as short-gauge sensors or long-gauge sensors. Long-gauge sensors measure average strain over the gauge lengths and are used for global monitoring of structures, in particular, those built of inhomogeneous materials. However, the strain distribution along the sensor's gauge length may be nonlinear and the measured average strain value that is commonly attributed to the midpoint of the sensor may be different from the real value of strain at that point. Consequently, excessively long sensors may feature significant errors in measurement. However, short-gauge sensors are more susceptible to other types of measurement error, most notably, error caused by discontinuities (open cracks) distributed in the monitored material. Thus an optimum gauge length is to be found. The error in average strain measurement inherent to the sensor's gauge length introduced by the strain distribution and discontinuities in the monitored material is modelled for the most common applications met in civil engineering practice. The modelling takes into account the geometric properties of the monitored structure and various load cases. Guidelines for the selection of an appropriate gauge length are proposed, and tables for measurement error estimation are presented.

Keywords: long-gauge sensors, measurement error, fibre-optic sensors, structural health monitoring, concrete and steel structures

1. Introduction

Many construction materials, particularly concrete, can be affected by local defects, such as cracks, air pockets and inclusions. All these defects introduce discontinuities in the mechanical material properties at a meso-level. More indicative for structural behaviour, however, are material properties at the macro-level. For example, although reinforced concrete consists of hardened cement paste matrix filled with aggregates of different sizes and steel reinforcing bars, reinforced concrete structures are mainly analysed at the macro-level as built of a virtually homogenous material—cracked reinforced concrete [1]. Therefore, for structural monitoring purposes it is necessary to use sensors that are insensitive to material discontinuities observed at the micro- and meso-levels while still providing reliable measurements at the macro-level. In other words, it is not of interest to know the exact strain in each component of the material—hardened cement paste, aggregate, and steel—but to evaluate the behaviour of the resulting material as a whole.

The availability of long-gauge fibre-optic sensors [2–4] has opened new and interesting possibilities for structural health monitoring. For example, long-gauge sensors based on low coherence interferometry allow the measurement of deformations over a measurement basis that can reach tens of metres with resolutions in the micrometre range. These sensors were proven to be applicable for monitoring at a global structural level through numerous projects [5]. The value of a measurement performed using a long-gauge sensor represents an average strain value along the sensor's gauge length, which is commonly attributed to the midpoint of the sensor. This is

illustrated in figure 1 and described as follows:

$$\varepsilon_{C,s} = \frac{\Delta L_s}{L_s} = \frac{u_B - u_A}{x_B - x_A} = \frac{1}{L_s}\int_{x_A}^{x_B} \varepsilon_{x,s}(x)\,\mathrm{d}x + \frac{1}{L_s}\sum_i \Delta w_{d,i}, \quad (1)$$

where A, B are points delimiting the gauge length of the sensor with coordinates x_A and x_B; C is the midpoint of the sensor with coordinate $x_C = (x_A + x_B)/2$; $L_s = x_B - x_A$ is the gauge length at reference time, before the deformation is applied; u_A, u_B are the x-axis component of displacements of points A and B after deformation is applied; $\varepsilon_{C,s}$ is the average strain at point C measured by the sensor; $\varepsilon_{x,s}(x)$ is the strain distribution along the x-axis of the sensor; and $\Delta w_{d,i}$ is the dimensional change of the ith ($x_i \in [x_A, x_B]$) discontinuity (crack opening, inclusion dimensional change, etc) in the direction of the x-axis, after the deformation is applied.

Equation (1) shows that the measured strain $\varepsilon_{C,s}$ depends on the strain distribution $\varepsilon_x(x)$ between points A and B, the number and the dimensional changes of discontinuities $\Delta w_{d,i}$ (size of crack openings or dimensional changes of inclusions) between points A and B, and the gauge length L_s. For nonlinear strain distribution between points A and B, the first term on the right-hand side of (1) is different from the real value of strain at point C, and this difference in general increases as the sensor's gauge length increases. Thus for more accurate measurements shorter sensors are needed. However, the accuracy of measurements of shorter sensors is affected by dimensional changes of discontinuities [6, 7]. Thus, an optimal gauge length is to be found as a compromise of the two requirements—it must be short enough to guarantee good accuracy of measurement for nonlinear strain distributions, but at the same time, long enough to guarantee good accuracy in the event of large dimensional changes of discontinuities. General recommendations for determining a sensor's gauge length and accuracy are given in the literature [5, 8], but an extensive analysis for the general case has not been performed, and directly applicable models and guidelines have not been presented. In this paper, the influence of the gauge length on measurement accuracy is examined, and the measurement error is modelled for prismatic beams subject to bending. The most frequent load cases—concentrated forces, and loads with polynomial distributions—are considered along with the most used materials in civil engineering—steel and concrete. Simplified guidelines are proposed for determining the optimal sensor gauge length given the geometrical properties of the structure.

2. Prismatic beams subject to bending

Prismatic beams have one dimension (length of a beam) that is significantly larger than the other two dimensions (width and depth). If the loads cause bending in only one plane, then the beam is called a 'plane beam', and the bending is called 'plane bending', otherwise the beam is called a 'spatial beam' and the bending is called 'spatial bending'. Spatial bending can be calculated as the superposition of plane bending in each of the perpendicular planes.

The cross-sectional geometric properties relevant for this study are the moment of inertia I, depth h and position of geometrical centroid (centre of gravity). The beams are represented by centrelines—lines connecting the geometrical centroids (centres of gravity) through the beam length. The beams typically carry loads perpendicular to the centreline and are subjected to bending. An example of a structure consisting of several beams with various cross-sectional properties and typical loads is presented in figure 2(*a*).

It is important to note in figure 2(*a*) that the beams are defined as 'free spans' between joints, where a joint is defined as points at which beams with different cross-sections or mutual angles different from 180° meet. Joints are marked with numbers in squares.

2.1. Loads

Loads can appear in the form of concentrated forces (e.g. vehicle on the bridge, F_y in figure 2(*a*)), concentrated external moments (e.g. transferred from other members, M_e in figure 2(*a*)), or distributed forces (e.g. weight of construction material or snow, q_y in figure 2(*a*)). Dead loads do not change intensity or position in time (weight of construction material). Live loads can change intensity and position along the structure (vehicle on the bridge or weight of snow). The loads generate internal forces in structural members—normal (axial) forces N, bending moments M, and shear forces V. In this study axially loaded members, columns, are not considered, but analysis for these members is similar to the analysis presented here for beams subjected to bending. Shear forces do not influence the sensor's measurement. Thus, the only internal force of interest is the bending moments whose distribution depends on the member's geometrical properties, the border conditions and the type of applied loads. An example of a bending moment distribution is given in figure 2(*b*).

2.2. Load–strain relation in elementary theory of beams

The strain fields in beams depend on the load type, the distribution of bending moments M, geometric properties of the cross sections and the mechanical properties of the construction material. In elementary beam theory (linear theory of the first order), four main assumptions are made: (i) strain is small (geometric linearity), (ii) deformation is small, (iii) Bernoulli's hypothesis is valid, and (iv) stress–strain relation is linear [9]. Assumptions (i)–(iii) are valid in general for beams with the length–depth (L/h) ratio higher than 5:1 [10], which is the case in common structures, while the validity of assumption (iv) depends on the properties of the construction material.

Structural steel has a linear stress–strain relation and the Young's modulus is a constant. Concrete has more complex behaviour and the Young's modulus depends on the magnitude of stress. For lower stresses the behaviour of concrete can be considered as linear, but for higher stresses this is not the case [1]. In order to simplify the presentation, the Young's modulus of concrete will be considered as constant regardless of the stress level; however this simplification is made only to abridge the presentation, and it does not affect general conclusions of

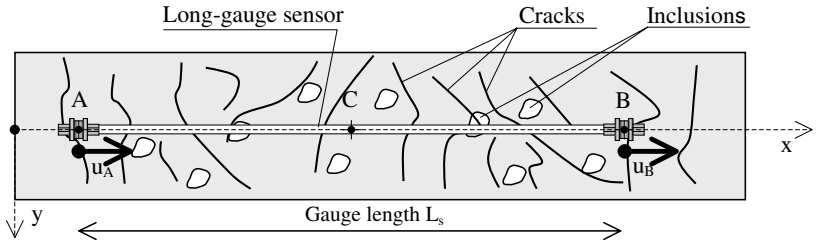

Figure 1. Schematic representation of a long-gauge sensor in an inhomogeneous material (courtesy of SMARTEC SA).

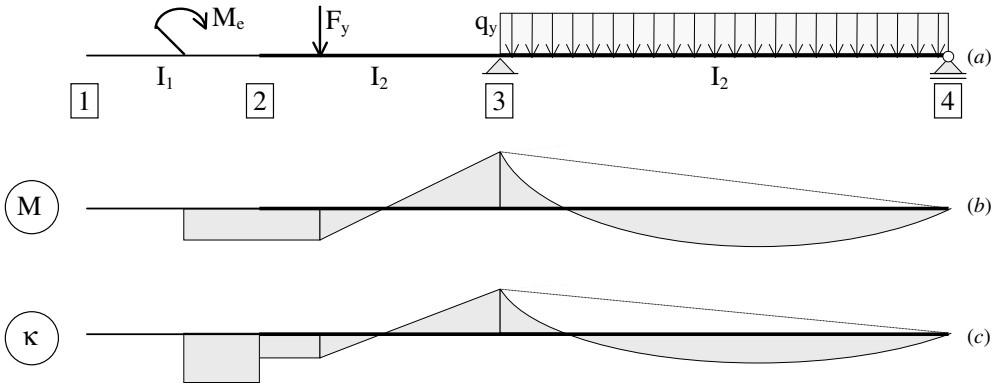

Figure 2. Schematic representation of a structure consisting of several beams subjected to bending loads, corresponding distribution diagrams of bending moments and cross-section curvatures.

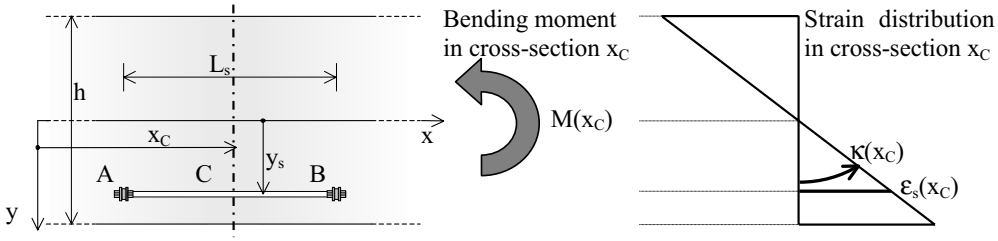

Figure 3. Strain distribution in the beam's cross-section.

the analysis. Provided that above-mentioned assumptions (i) to (iv) are valid, the distribution of strain ε_x in a beam subject to bending is given by the following expression:

$$\varepsilon_x(x, y) = \frac{M(x)}{E \cdot I} \cdot y = \kappa(x) \cdot y, \tag{2}$$

where E is the Young's modulus of the construction material (constant) and $\kappa(x)$ is the curvature in a cross-section.

Let a long-gauge sensor be installed at a distance y_s from the centre of gravity as shown in figure 3.

The expected strain at the midpoint of the sensor is calculated using (2) by substituting x and y with x_C and y_s. The strain distribution along the beam is obtained by substituting y with y_C. Curvature in a cross-section is a direct consequence of a bending moment and is therefore a deformation parameter that is relevant to bending. An example of the distribution of curvature in a structure consisting of several beams is given in figure 2(*c*).

2.3. Saint-Venant principle

Concentrated loads, forces and moments, as well as distributed loads with abrupt changes along the beam create perturbations of stress and strain which make (2) inapplicable. The Saint-Venant principle states that at points 'far enough' from the point of perturbation, the stress and strain fields comply with (2). Theoretical derivations and experimental results demonstrated that in most cases the 'safe' distance for common cross-sections corresponds to the depth h of the beam [10]. Consequently, (2) can be used only for parts of the girders subjected to a 'smooth' distributed load that are approximately a distance h away from the location where the loads are applied (including the extremities of the structural member). Otherwise, a correction factor is to be added [10].

3. Influence of the gauge length on the accuracy of measurement

In order to assess the influence of the sensor's gauge length on the accuracy of the measurement, it is necessary to split the problem into several basic load cases as shown in table 1. The case IDs are composed as follows: first letter B = beam; second letter for sensors installed far from extremities: E = load at extremities, P = polynomial load distribution along the structural member, F = concentrated load, M = concentrated

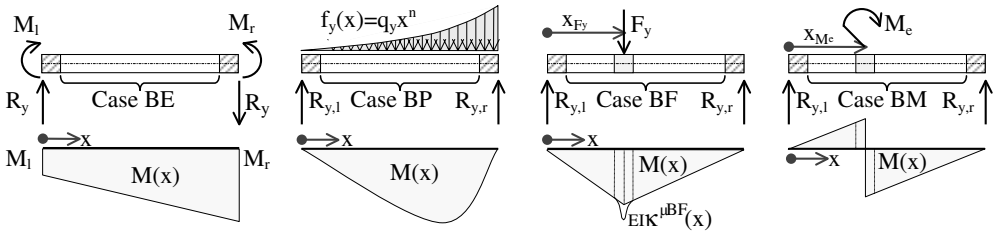

Figure 4. Basic load cases and the corresponding distribution of bending moments.

Table 1. Breakdown of the problem.

Case ID	Structural member	Load type	Position of the sensor
BE	Beam	At the extremities of the structural member	Far from extremities
BP	Beam	Polynomial load along the structural member	Far from extremities
BF	Beam	Concentrated force	Far from extremities
BM	Beam	Concentrated moment	Far from extremities
BX	Beam	Any	Close to extremities

moment; second letter X for any type of load installed close to extremities. The basic load cases and the corresponding diagrams of bending moments are given in figure 4.

Once the influence on each basic load case has been determined, complex cases can be solved using the principle of superposition. For example, the accuracy of the sensors installed in structural members 2 and 3 in figure 2 can be analysed as a combination of basic cases BE and BF for sensors far from joints 2 and 3. For sensors installed close to the extremities, case BX can be added.

The analysis is performed separately for homogeneous and inhomogeneous materials. For a homogeneous material, the average strain measured by the sensor which is attributed to the sensor's midpoint is given by the first term (integral) on the right-side part of (1). The error of measurement inherent to the gauge length is calculated as follows:

$$\begin{aligned}\delta\varepsilon_{C,s} &= \varepsilon_{C,s} - \varepsilon_x(x_C, y_s)\\ &= \frac{1}{L_s}\int_{x_A}^{x_B}\frac{M(x)}{E\cdot I}y_s\,\mathrm{d}x - \frac{M(x_C)}{E\cdot I}\cdot y_s\\ &= \frac{y_s}{E\cdot I}\left(\frac{1}{L_s}\int_{x_A}^{x_B}M(x)\,\mathrm{d}x - M(x_s)\right).\end{aligned} \tag{3}$$

For an inhomogeneous material the second term (sum) of the same expression is corrected as shown in section 3.7.

3.1. Homogeneous structural member loaded at extremities (case BE)

For structural members loaded at the extremities as shown in figure 4, the bending moment distribution function is given as follows:

$$M(x) = M_l + R_y x = M_l + \frac{M_r - M_l}{L_{\text{beam}}}x, \tag{4}$$

where L_{beam} is the length of the beam.

The error of the measurement inherent to the gauge length is obtained by combining (3) and (4), and taking into account that $x_C = (x_A + x_B)/2$ and $L_s = x_B - x_A$ (see figure 1 and (1)):

$$\delta\varepsilon_{C,s} = \frac{y_s}{E\cdot I}\left\{\frac{1}{x_B - x_A}\left[\left(M_l x_B + R_y\frac{x_B^2}{2}\right) - \left(M_l x_A + R_y\frac{x_A^2}{2}\right)\right] - \left(M_l + R_y\frac{x_A + x_B}{2}\right)\right\} = 0. \tag{5}$$

Consequently, the gauge length does not affect the accuracy of the sensors for structural members loaded at the extremities if the sensors are installed 'far enough' from the extremities.

3.2. Homogeneous beam loaded with distributed loads (case BP)

For a homogeneous beam loaded with a distributed load as shown in figure 4, the resultant force is expressed in (6*a*) and the bending moment distribution function is given in (6*b*), taking into account the equilibrium conditions between the loads and reactions at extremities:

$$F_{R_y} = \int_0^L q_y x^n\,\mathrm{d}x = q_y\frac{L_{\text{beam}}^{n+1}}{n+1}; \tag{6a}$$

$$M(x) = \frac{q_y}{(n+1)(n+2)}\left(L_{\text{beam}}^{n+1}x - x^{n+2}\right). \tag{6b}$$

The relation between the maximal moment $M_{\max}^{\text{BP}}$ and maximal strain $\varepsilon_{\max}^{\text{BP}}$ for case BP is found using the local maximum of the function defined in (3) combined with (6*b*):

$$\begin{aligned}\varepsilon_{\max}^{\text{BP}} &= \frac{y_s}{E\cdot I}M_{\max}^{\text{BP}} = \frac{y_s}{E\cdot I}q_y\frac{L_{\text{beam}}^{n+2}}{n+1}\alpha_n\\ &= \frac{y_s}{E\cdot I}F_{R_y}L_{\text{beam}}\alpha_n,\end{aligned} \tag{7}$$

where $\alpha_n = \frac{n+1}{(n+2)^{2}\cdot\sqrt[n+1]{n+2}}$.

The error of the measurement inherent to the gauge length in the case of bending is obtained by combining equations (3), (6*a*) and (7) taking into account that $x_C = (x_A + x_B)/2$ and $L_s = x_B - x_A$ (see figure 1 and (1)):

$$\delta\varepsilon_{C,s}^{\text{BP}} = -\frac{y_s}{E\cdot I}\cdot\frac{F_{R_y}}{(n+2)(n+3)L^{n+1}} \times\sum_{i=0}^{n+1}\left[\binom{n+3}{i}\frac{1-(-1)^{n+3-i}}{2^{n+3-1}}\right]L_s^{n+2-i}x_C^i. \tag{8}$$

This equation demonstrates that in general the error in the measurement exponentially depends on the sensor's gauge length L_s and, for $n > 0$, on the position x_C. In order to further

Table 2. Coefficients $\phi^{\mathrm{BP},n}$.

ξ	$n=0$	$n=1$	$n=2$	$n=3$	$n=4$	$n=5$	$n=6$	$n=7$	$n=8$	$n=9$	$n=10$
1/20	−0.001	−0.002	−0.003	−0.004	−0.005	−0.006	−0.008	−0.009	−0.011	−0.013	−0.015
1/10	−0.003	−0.006	−0.010	−0.013	−0.018	−0.022	−0.026	−0.031	−0.036	−0.041	−0.046
1/8	−0.005	−0.010	−0.015	−0.020	−0.026	−0.032	−0.038	−0.045	−0.051	−0.057	−0.063
1/6	−0.009	−0.017	−0.025	−0.033	−0.042	−0.051	−0.060	−0.068	−0.076	−0.084	−0.091
1/5	−0.013	−0.023	−0.034	−0.046	−0.057	−0.068	−0.078	−0.087	−0.096	−0.104	−0.111
1/4	−0.021	−0.036	−0.051	−0.066	−0.080	−0.092	−0.104	−0.114	−0.122	−0.129	−0.135
1/3	−0.037	−0.060	−0.082	−0.101	−0.118	−0.131	−0.142	−0.150	−0.155	−0.159	−0.161
1/2	−0.083	−0.122	−0.150	−0.170	−0.181	−0.186	−0.187	−0.185	−0.180	−0.174	−0.167
3/4	−0.188	−0.228	−0.241	−0.237	−0.225	−0.209	−0.192	−0.176	−0.161	−0.147	−0.135
1	−0.333	−0.325	−0.291	−0.253	−0.218	−0.189	−0.165	−0.145	−0.129	−0.116	−0.105

evaluate the measurement error, (8) can be transformed by numerical transformations and substitution with (7):

$$\delta\varepsilon^{\mathrm{BP}}_{C,s} = -\frac{\varepsilon^{\mathrm{BP}}_{\max}}{\alpha_n(n+2)(n+3)} \times \frac{1}{\xi}\left[\left(\eta+\frac{\xi}{2}\right)^{n+3} - \left(\eta-\frac{\xi}{2}\right)^{n+3} - (n+3)\xi\eta^{n+2}\right], \quad (9)$$

where $\xi = \frac{L_s}{L_{\mathrm{beam}}}$ and $\eta = \frac{x_C}{L_{\mathrm{beam}}}$.

As per (8), the biggest error in the measurement is obtained for the maximal x_C, which is less than or equal to $L_{\mathrm{beam}} - L_s/2$ (i.e. $\eta \leqslant 1 - \xi/2$). With this substitution in (9), the maximal absolute error can be estimated as

$$\left|\delta\varepsilon^{\mathrm{BP}}_{C,s}\right| \leqslant \varepsilon^{\mathrm{BP}}_{\max}\left|\phi^{\mathrm{BP},n}\right|, \qquad \phi^{\mathrm{BP},n} = -\frac{1}{\alpha_n(n+2)(n+3)} \times \frac{1}{\xi}\left[1-(1-\xi)^{n+3} - (n+3)\xi\left(1-\frac{\xi}{2}\right)^{n+2}\right]. \quad (10)$$

The coefficients $\phi^{\mathrm{BP},n}$ are given in table 2. They represent a relative error in the measurement of maximal strain and can be used as a criterion to determine the maximal gauge length of a sensor.

For example, let $n = 2$ and let the criterion be to measure the maximal strain with relative error not exceeding 1% (=0.01); then the sensor's gauge length should not exceed 1/10 of the length of the beam (see table 2).

For the most common case, $n = 0$, uniformly distributed load (dead weight, snow, etc), and $n = 1$, linearly distributed load, the error is calculated as follows:

$$n=0 \Rightarrow f_y(x) = q_y = \mathrm{const} \Rightarrow \delta\varepsilon^{\mathrm{BP}}_{C,s} = -\frac{y_s}{E\cdot I}\frac{q_y L_s^2}{24} = -\frac{y_s}{E\cdot I}\frac{F_{R_y}}{L_{\mathrm{beam}}}\frac{L_s^2}{24} = -\frac{1}{3}\varepsilon^{\mathrm{BP}}_{\max}\xi^2, \quad (11a)$$

$$n=1 \Rightarrow f_y(x) = q_y x \Rightarrow \delta\varepsilon^{\mathrm{BP}}_{C,s} = -\frac{y_s}{E\cdot I}\frac{q_y L_s^2}{24}x_C = -\frac{y_s}{E\cdot I}\frac{F_{R_y}}{L_{\mathrm{beam}}^2}\frac{L_s^2}{12}x_C = -0.650\varepsilon^{\mathrm{BP}}_{\max}\xi^2\eta. \quad (11b)$$

The relative error in the measurement of maximal strain does not exceed 1% for $L_s \leqslant L_{\mathrm{beam}}/6$ in the case of uniformly distributed load ($n = 0$) and for $L_s \leqslant L_{\mathrm{beam}}/8$ in the case of linearly distributed load ($n = 1$).

3.3. Homogeneous beam loaded with concentrated force (case BF)

For a homogeneous beam loaded with concentrated force as shown in figure 4, the bending moment diagram has a 'broken line' shape. The force application cross-section splits the beam into two segments, and each segment can be considered as a beam loaded at the extremities, see figure 4. Consequently, the sensors installed 'far enough' from the force application cross-section are exposed to the linear distribution of strain as in case BE, and the gauge length does not involve error in measurement (see subsection 3.1).

For the cross-sections close to the application point of the force, the strain distribution is more complex and does not follow (2) [10, 11]. In general the strain field can be presented as a sum of the strain field from (2), superposed with the corrective strain field $\varepsilon^{\mu^{\mathrm{BF}}}(x, y)$ [10], i.e.,

$$\varepsilon_x(x,y) = \frac{M^{\mathrm{BF}}(x)}{E\cdot I}\cdot y + \varepsilon^{\mu^{\mathrm{BF}}}(x,y) = \kappa^{M^{\mathrm{BF}}}(x)\cdot y + \varepsilon^{\mu^{\mathrm{BF}}}(x,y), \quad (12)$$

where

$$M^{\mathrm{BF}}(x) = \left\{ F_y\left(1-\frac{x_{F_y}}{L_{\mathrm{beam}}}\right)x \,\middle|\, x \leqslant x_{F_y},\ F_y x_{F_y}\left(1-\frac{x}{L_{\mathrm{beam}}}\right) \,\middle|\, x \geqslant x_{F_y}\right\}$$

and x_{F_y} is the coordinate of the force application cross-section.

The measurement error relative to the first term of (12) depends on the position of the sensor. The maximal measurement error is generated when the sensor's midpoint corresponds to the force application cross-section [5]. In this case, the maximal strain at the sensor's midpoint, relative to the first term on the right-hand side of (12), is given in (13) and the maximal error in (14):

$$\varepsilon^{M^{\mathrm{BF}}}_{\max} = \frac{M^{\mathrm{BF}}(x_{F_y})}{E\cdot I}\cdot y_s = \frac{F_y y_s}{E\cdot I}x_{F_y}\left(1-\frac{x_{F_y}}{L_{\mathrm{beam}}}\right) = \frac{F_y y_s}{E\cdot I}L_{\mathrm{beam}}\eta_{F_y}\left(1-\eta_{F_y}\right), \quad (13)$$

$$\delta\varepsilon^{M^{\mathrm{BF}}}_{C,s} = -\frac{1}{8}\frac{F_y y_s}{E\cdot I}L_s = -\frac{1}{8}\varepsilon^{M^{\mathrm{BF}}}_{\max}\frac{\xi}{\eta_{F_y}\left(1-\eta_{F_y}\right)}. \quad (14)$$

The influence of the gauge length on the second term of (12) is more difficult to determine, since the function $\varepsilon^{\mu^{\mathrm{BF}}}(x, y)$ varies

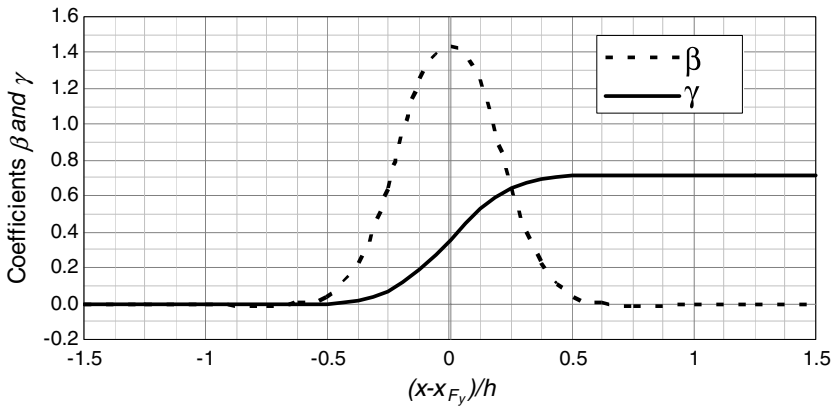

Figure 5. Functions β and γ.

significantly along the x-axis (changes sign) and is nonlinear along the y-axis [10]. The Bernoulli hypothesis is not valid in the strain perturbation zone (cross-section does not remain a plane after the deformation) and (2) is not valid. However, the real values of the strain in the cross-sections close to the force application point are not of interest for global structural monitoring, and rather an overall deformation created by a strain field perturbation is of interest. The estimation of this global influence requires more sophisticated analysis that exceeds the scope of this research. Only the most common case is analysed—a beam with a rectangular cross-section with a force applied on an external surface. In order to evaluate the error due to the gauge length, let us define equivalent strain as the strain value assuming that the Bernoulli hypothesis is valid, i.e. the cross-sections remain a plane after deformation. The equivalent strain and the curvature correction around the force application cross-section [10] are then expressed as follows (respectively):

$$\varepsilon_{\text{equ}}^{\mu^{\text{BF}}}(x,y) = \kappa^{\mu^{\text{BF}}}(x)\cdot y = \left[\frac{1}{h}\int_h \frac{\varepsilon^{\mu^{\text{BF}}}(x,y)}{y}\,\mathrm{d}y\right]\cdot y, \qquad (15a)$$

$$\kappa^{\mu^{\text{BF}}}(x) = \frac{1}{3}\beta\left(\frac{x-x_{F_y}}{h}\right)\frac{F_y h}{E\cdot I}, \qquad (15b)$$

where h is the depth of the cross-section and β is the function dependent on x as shown in figure 5.

The equivalent strain is different from real strain, but it gives equivalent global deformation as the real strain, i.e. the same curvature and deformed shape. Maximal equivalent strain at the location of the sensor is obtained by combining (2) and (15b) for $x = x_{F_y}$ and $\beta = 1.438$ (figure 5), and presented as follows:

$$\begin{aligned}\varepsilon_{\text{equ,max}}^{\mu^{\text{BF}}} &= 0.479\frac{F_y h}{E\cdot I}y_s \\ &= 0.479\varepsilon_{\text{max}}^{M^{\text{BF}}}\frac{h}{L_{\text{beam}}}\frac{1}{\eta_{F_y}(1-\eta_{F_y})}.\end{aligned} \qquad (16)$$

According to figure 5, when the cross-section of interest is approximately $0.5h$ from the cross-section where the force is applied, the corrective curvature is close to zero. Thus, the Bernoulli hypothesis is valid at that point and the strain field is approximately equal to the field as determined in the elementary theory of beams. For sensors with a gauge length shorter than h, the above statements are not valid and the use of such a short sensor is not recommended. Because measurements depend on a sensor's position in the cross-section, the results may be difficult to interpret. That is why sensors with a gauge length not shorter than the depth of the cross-section h are recommended for structural monitoring, and only these sensors are analysed further in this text. The measurement of the sensor with a gauge length not shorter than the depth of the cross-section (i.e. $L_s \geqslant h$) is expressed as

$$\begin{aligned}\varepsilon_{C,s}^{\mu^{\text{BF}}} &= \frac{1}{3}\frac{F_y h}{E\cdot I}y_s\frac{1}{\left(\frac{x_B-x_{F_y}}{h}-\frac{x_A-x_{F_y}}{h}\right)} \\ &\quad\times\int_{\frac{x_A-x_{F_y}}{h}}^{\frac{x_B-x_{F_y}}{h}}\beta\left(\frac{x-x_{F_y}}{h}\right)\mathrm{d}x \\ &= 0.695\varepsilon_{\text{equ,max}}^{\mu^{\text{BF}}}\frac{h}{L_s}\left[\gamma\left(\frac{L_s}{2h}\right)-\gamma\left(-\frac{L_s}{2h}\right)\right],\end{aligned} \qquad (17)$$

where γ is the integral of β, dependent on x as shown in figure 5.

It can be noticed in figure 5 that for values $L_s \geqslant h$ the function γ is constant for $(x-x_{F_y})/h \geqslant 0.5$ and approximately equal to 0.715, and for $(x-x_{F_y})/h \leqslant -0.5$ it is approximately equal to 0. Thus, for $L_s \geqslant h$, (17) transforms into (18) and the measurement error is estimated using (19):

$$\begin{aligned}\varepsilon_{C,s}^{\mu^{\text{BF}}} &= 0.497\varepsilon_{\text{equ,max}}^{\mu^{\text{BF}}}\frac{h}{L_s} \\ &= 0.238\varepsilon_{\text{max}}^{M^{\text{BF}}}\frac{h^2}{L_{\text{beam}}L_s}\frac{1}{\eta_{F_y}(1-\eta_{F_y})};\end{aligned} \qquad (18)$$

$$\begin{aligned}\delta\varepsilon_{C,s}^{\mu^{\text{BF}}} &= \varepsilon_{\text{equ,max}}^{\mu^{\text{BF}}}\left(0.497\frac{h}{L_s}-1\right) \\ &= \varepsilon_{\text{max}}^{M^{\text{BF}}}\frac{h}{L}\frac{1}{\eta_{F_y}(1-\eta_{F_y})}\left(0.238\frac{h}{L_s}-0.479\right).\end{aligned} \qquad (19)$$

Equation (19) is used to assess the error generated by a strain field perturbation for $L_s \geqslant h$. It is important to highlight that this error does not depend on the position of the force. For example, for $L_s = h$ the error is equal to 0.503 of the maximal equivalent strain (from (19)). Finally, the maximal equivalent strain and the corresponding error are calculated

Table 3. Coefficients ϕ^{BF}.

	$L_s = h$			$L_s = 1.5h$			$L_s = 2h$			$L_s = 3h$		
h/L_{beam}	ξ	$\eta_{F_y} = \frac{1}{2}$	$\eta_{F_y} = \frac{1}{4}$	ξ	$\eta_{F_y} = \frac{1}{2}$	$\eta_{F_y} = \frac{1}{4}$	ξ	$\eta_{F_y} = \frac{1}{2}$	$\eta_{F_y} = \frac{1}{4}$	ξ	$\eta_{F_y} = \frac{1}{2}$	$\eta_{F_y} = \frac{1}{4}$
1/40	1/40	−0.035	−0.046	1/26.7	−0.048	−0.064	1/20	−0.058	−0.076	1/13.3	−0.074	−0.097
1/30	1/30	−0.046	−0.060	1/20	−0.064	−0.083	1/15	−0.076	−0.100	1/10	−0.097	−0.127
1/25	1/25	−0.054	−0.071	1/16.7	−0.075	−0.098	1/12.5	−0.091	−0.118	1/8.3	−0.115	−0.150
1/20	1/20	−0.067	−0.087	1/13.3	−0.093	−0.120	1/10	−0.111	−0.144	1/6.7	−0.141	−0.183
1/15	1/15	−0.087	−0.111	1/10	−0.120	−0.154	1/7.5	−0.144	−0.185	1/5	−0.183	−0.235
1/10	1/10	−0.123	−0.155	1/6.7	−0.170	−0.216	1/5	−0.205	−0.259	1/3.3	−0.260	−0.329
1/8	1/8	−0.148	−0.185	1/5.3	−0.205	−0.257	1/4	−0.246	−0.308	1/2.7	−0.312	−0.391
1/6	1/6	−0.185	−0.228	1/4	−0.257	−0.317	1/3	−0.308	−0.380	1/2	−0.391	−0.483
1/5	1/5	−0.212	−0.258	1/3.3	−0.294	−0.359	1/2.5	−0.353	−0.431	1/1.7	−0.448	−0.547

Table 4. Coefficients ϕ^{BF}_{left} and ϕ^{BF}_{right}.

	$L_s = 0.5h$				$L_s = 0.75h$				$L_s = h$			$L_s = 1.5h$		
$\eta_{F_y} =$		$\frac{1}{2}$		$\frac{1}{4}$		$\frac{1}{2}$		$\frac{1}{4}$	$\frac{1}{2}$		$\frac{1}{4}$	$\frac{1}{2}$		$\frac{1}{4}$
h/L_{beam}	ξ	Both	Left	Right	ξ	Both	Left	Right	Both	Left	Right	Both	Left	Right
1/40	1/80	0.007	0.009	0.009	1/53	0.026	0.035	0.035	0.033	0.045	0.043	0.026	0.036	0.034
1/30	1/60	0.009	0.012	0.012	1/40	0.035	0.048	0.046	0.044	0.061	0.058	0.035	0.049	0.046
1/25	1/50	0.011	0.015	0.015	1/33	0.042	0.058	0.056	0.053	0.074	0.070	0.042	0.060	0.055
1/20	1/40	0.014	0.019	0.018	1/27	0.053	0.074	0.070	0.067	0.095	0.088	0.054	0.078	0.070
1/15	1/30	0.019	0.026	0.024	1/20	0.072	0.101	0.094	0.092	0.131	0.119	0.074	0.110	0.095
1/10	1/20	0.028	0.040	0.037	1/13	0.110	0.160	0.143	0.142	0.214	0.183	0.117	0.189	0.147
1/8	1/16	0.036	0.051	0.047	1/11	0.141	0.210	0.182	0.183	0.285	0.233	0.153	0.265	0.189
1/6	1/12	0.049	0.072	0.063	1/8	0.195	0.303	0.248	0.256	0.427	0.320	0.221	0.441	0.265
1/5	1/10	0.060	0.090	0.077	1/7	0.240	0.389	0.303	0.320	0.569	0.394	0.284	0.662	0.331

by combining equations (13) and (18), and equations (14) and (19) respectively, as follows:

$$\varepsilon^{BF}_{max} = \varepsilon^{M^{BF}}_{max} + \varepsilon^{\mu^{BF}}_{equ,max} = \varepsilon^{M^{BF}}_{max}\left[1 + 0.479\frac{h}{L_{beam}}\frac{1}{\eta_{F_y}\left(1-\eta_{F_y}\right)}\right]; \tag{20}$$

$$\delta\varepsilon^{BF}_{C,s} = \delta\varepsilon^{M^{BF}}_{C,s} + \delta\varepsilon^{\mu^{BF}}_{C,s} = \varepsilon^{M^{BF}}_{max}\frac{1}{\eta_{F_y}\left(1-\eta_{F_y}\right)} \times \left[\frac{h}{L}\left(0.238\frac{h}{L_s} - 0.479\right) - \frac{1}{8}\frac{L_s}{L_{beam}}\right] = \varepsilon^{M^{BF}}_{max}\phi^{BF}. \tag{21}$$

These equations help determine the magnitude of the measurement error with respect to the total equivalent strain generated by the concentrated force. The measurement error for the concentrated force acting in the middle and at quarter of the span are given for various ratios h/L_{beam} and h/L_s ($L_s \geqslant h$) in table 3.

In common practice, the ratio h/L_{beam} is for steel structures between $L_{beam}/20$ and $L_{beam}/30$ and for reinforced concrete girders between 1/15 and 1/25. For these girders it is recommended to use a gauge length not exceeding $1.5h$ in order keep the relative error contained between 5% and 15% (reinforced concrete is not a homogeneous material, but this observation is given here as information to be considered later in the text). The ratio h/L_{beam} is much smaller for pre-stressed or post-tensioned girders, between 1/30 and 1/40, and longer gauge lengths can be used.

Using the equations presented in this section it can be proven that the accuracy of measurement can be significantly improved if the sensor with the gauge length L_s is replaced with two shorter sensors with gauge lengths equal to $L_{s,half} = L_s/2$, installed to the left and right of the force application cross-section. In this case, the result of monitoring provides two values of measured strain at distances $-L_{s,half}/2$ and $+L_{s,half}/2$ from the force application cross-section. The total error in measurement inherent to the gauge length is calculated using equations (12)–(17) with appropriate substitution of coordinates. In order to simplify the presentation, the derivation of these formulae is not presented, but final results are as follows:

$$\delta\varepsilon^{BF,left}_{C,s,half} = \varepsilon^{M^{BF}}_{C,half}(x_{C,half})\phi^{BF}_{left}; \tag{22a}$$

$$\delta\varepsilon^{BF,right}_{C,s,half} = \varepsilon^{M^{BF}}_{C,half}(x_{C,half})\phi^{BF}_{right}. \tag{22b}$$

The coefficients ϕ^{BF}_{left} and ϕ^{BF}_{right} are given in table 4.

The values presented in table 4 are in general smaller than those presented in table 3. Consequently, if the position of the concentrated force on the beam is known (e.g. support 3 in figure 2), then it is recommended to use two sensors installed on each side of the force application cross-section and to determine the length of the sensors based on (22*b*) and table 4. However, the position of the force is frequently not pre-defined (e.g. a vehicle on the bridge), and in that case it is recommended to use sensors with gauge lengths determined using (21) and table 3.

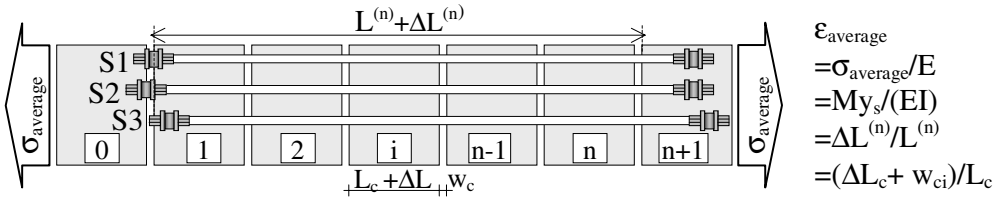

Figure 6. Schematic representation of the influence of the discontinuities on the sensor measurement.

3.4. Homogeneous beam loaded with concentrated moment (case BM)

A concentrated moment creates a discontinuity in the bending moment distribution (bending moment diagram), as shown in figure 4. The bending moment distribution 'far enough' from the extremities and 'far enough' from the moment application cross-section is linear, and the error in measurement inherent to the gauge length is null (see section 3.2). The bending moment diagram practically has two values at the cross-section where the concentrated moment is applied, one on the left and the other on the right of the application cross-section. Consequently two sensors installed at these positions are to be used for monitoring. This solution is possible only if the concentrated moment acts as a dead load, i.e. if it does not change position, which in real cases occurs when the moment is transferred to the beam from some other structural member. However, in that situation, the interception point between the loading structural member and the beam defines the extremity of the beam and the moment application cross-section is practically at the extremity. This case is discussed in the next subsection. Live loads can also create concentrated moments (e.g. heavy vehicle that suddenly brakes), but since their position is not pre-defined on the beam, the strain they generate at the application cross-section cannot be directly measured, since the position where the required pair of sensors is to be installed is not known. Thus, no specific recommendation for determining the gauge length can be proposed, except to keep it longer than or equal to the depth of the cross-section in order to overcome issues related to local strain perturbations.

3.5. Cross-sections close to the extremities of a homogeneous beam (case BX)

The strain field in the cross-sections close to the extremities of the beam is perturbed due to concentrated loads and does not in general conform to predictions made by the elementary theory of beams. It depends strongly on border conditions, which is why a simple and universal solution for modelling the stain perturbation does not exist. Consequently, it is impossible to model the error of measurement inherent to the gauge length for the sensors installed close to the extremities in a simplified manner. The general recommendation is to use a sensor with the gauge length at least as long as the cross-section depth. In the cases where the concentrated force acts at the extremity of the beam (and models developed in subsection 3.3 are valid), then the gauge length of the sensor can be decreased to one half of the cross-section depth. Another solution is to use sensors with a gauge length determined using other criteria presented in this paper, but to position the sensors 'far enough' from the extremities.

3.6. Inhomogeneous beam

Reinforced concrete structures, although truly inhomogeneous (at meso-level), are considered as homogeneous (at macro-level) during design and structural analysis. The idea of using long-gauge sensors follows the philosophy of reinforced concrete: the structural condition of an inhomogeneous material is assessed considering it as a homogeneous material.

In an ideally homogeneous material, without local defects or discontinuities (cracks), the elastic strain field follows the theoretical models; thus in an ideally homogeneous material the use of a short gauge length is not an issue (except at locations of concentrated loads). In contrast, in inhomogeneous materials and notably materials with discontinuities (e.g. cracks in reinforced concrete) sensors with a short gauge length cannot be used for monitoring at the structural level [7, 12].

Let us observe three sensors with equal gauge lengths installed in a plane at a distance y_s from the centreline, as shown in figure 6 (plane view). Let the sensor position in the plane be as follows: two sensors have extremities belonging to the same cross-sections ($S1$ and $S2$), while the third sensor ($S3$) is slightly shifted along the x-axis (see figure 6). Finally, let us suppose that the beam is built of reinforced concrete, sensors are installed in the tensioned part of the beam, and, to simplify presentation, the average strain is constant along the sensors (e.g. the bending moment diagram is constant). Due to tension, the reinforced concrete element will crack; let us suppose that the first crack occurs exactly in one of the cross-sections where $S1$ and $S2$ have their extremities. In the worst case, the extremities of the sensors will belong to two separate blocks of concrete, as shown in figure 6. The sensor $S3$ is only slightly axially shifted; thus its left extremity belongs to block 1. The other extremities of all three sensors belong to the same block $n + 1$.

Since the theoretical average strain field in the beam is constant, all three of the sensors are expected to measure this same value. However, due to cracking and imperfection in the sensor positions, the measurements of sensors $S1$, $S2$ and $S3$ will be different from each other and from the calculated average strain in the beam. This error is analysed in [5] and presented as follows where the notation is as given in figure 6:

$$\delta\varepsilon_{C,s}^{\text{crack}} \approx \pm\frac{w_c}{L_s} \approx \pm\varepsilon_{C,s}\frac{w_c}{\Delta L_c + w_c}\cdot\frac{L_c}{L_s} < \pm\varepsilon_{C,s}\frac{L_c}{L_s} = \pm\varepsilon_{C,s}\phi^{\text{crack}}; \tag{23}$$

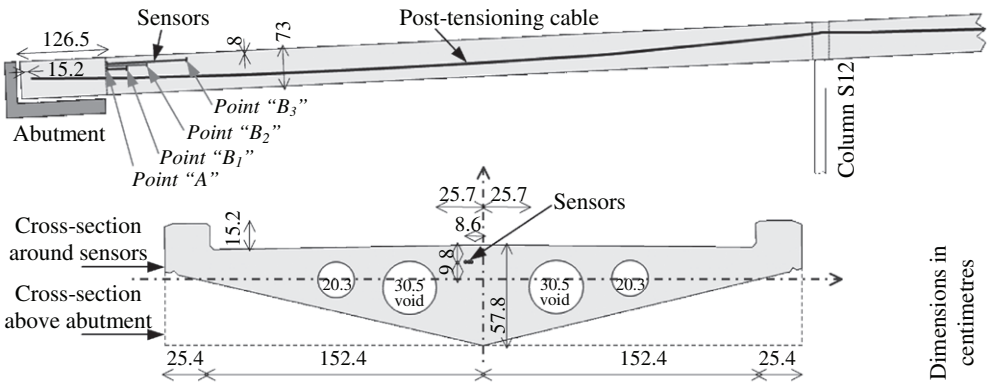

Figure 7. Position of the sensors in the structure.

This equation demonstrates that a longer length of the sensor's gauge length provides results with lower errors and consequently with better accuracy in the measurements. To achieve a relative error smaller than 10%, it is necessary to use sensors that are at least ten times longer than the distance between the cracks L_c. In order to improve the durability of concrete structures, it is preferred to have larger number of cracks along the beam with a low crack width, instead of having fewer cracks with large widths. A typical spacing between the cracks ranges between 100 and 300 mm [13], and consequently typical minimal recommended lengths of sensors range between 1 and 3 m.

If the gauge length is shorter than the distance between the cracks, then, depending on position, the sensor will either measure strain in the tensioned concrete, which is much lower than the calculated average strain in the beam, or measure the ratio between crack opening and gauge length, which is much higher than the calculated average strain in the beam [5]. These results are interesting from the point of view of local material behaviour, but they do not provide information on global structural behaviour.

3.7. Combined loading

A beam is, in general, subjected to a combination of distributed and concentrated loads. For beams that behave in accordance with elementary beam theory, the strain generated by a combination of loads can be presented as the sum of strain generated by each individual load. Thus, in the general case, the combined strain and the limits of measurement error for a given gauge length are calculated as follows:

$$\varepsilon_{C,s}^{\text{comb.}} = \sum_i \varepsilon_{C,s,i}^{\text{BE}} + \sum_j \varepsilon_{C,s,j}^{\text{BP}} + \sum_k \varepsilon_{C,s,k}^{\text{BF}}; \tag{24a}$$

$$\delta\varepsilon_{C,s}^{\text{comb.}} = \sum_i \delta\varepsilon_{C,s,i}^{\text{BE}} + \sum_j \delta\varepsilon_{C,s,j}^{\text{BP}} + \sum_k \delta\varepsilon_{C,s,k}^{\text{BF}} \pm \delta\varepsilon_{C,s}^{\text{crack}}. \tag{24b}$$

In (24*b*) the term related to case 'BE' is null, and the term related to case 'BF' is also null if the sensor is far enough from the force application cross-section.

4. Case study—comparison of measurement by sensors with different gauge lengths

The southeast leg (SE-leg) of the Streicker Bridge at Princeton University campus is a curved continuous girder made of post-tensioned concrete and supported by weathering steel columns [15]. The bridge has been equipped with Bragg-grating fibre-optic long-gauge sensors [15] with absolute measurement error estimated to be 4 $\mu\varepsilon$ (4×10^{-6} m/m). The monitoring project has broad research and education aims, but only a part of the research relevant to the topic of this paper is presented here, while more details about the other aims of the project, the employed monitoring strategy and the monitoring system are found in the literature [15, 16]. The aim of this section is to present the differences in measurements obtained by sensors with different gauge lengths, installed in the zone where the strain field is perturbed.

In order to assess the influence of the gauge length on the average strain measurement, three sensors AB_1, AB_2, and AB_3, with gauge lengths $L_{AB1} = 0.3$ m, $L_{AB2} = 0.6$ m, and $L_{AB3} = 1.2$ m, respectively, were embedded in concrete close to each other, at the same distance from the centre of gravity, parallel to the elastic line of the beam, in the zone with constant cross-section, as shown in figure 7. The bridge has horizontal curvature, but radius (110 m) is several orders of magnitude bigger than the length of sensors; thus the bridge can locally be considered as prismatic. The sensors were close to the abutment, in the zone where the strain field was expected to be perturbed by the proximity of the concentrated reaction force from the abutment, and the change in cross-sectional properties.

The post-tensioning of the SE-leg was performed in three stages by applying approximately 25%, 55% and 100% of the full post-tensioning force. Measurements were made three times in the first two stages, and four times in the last stage. The results of the measurements are presented in figure 8 as discrete spots. The strain distribution at the location of sensors is calculated theoretically for each stage based on simplified elastostatics theory [10]. The theoretically calculated strain distributions are presented in figure 8 in the form of continuous or dashed lines.

The measurement error inherent to the gauge length could not be accurately determined for the following reasons: (I) no

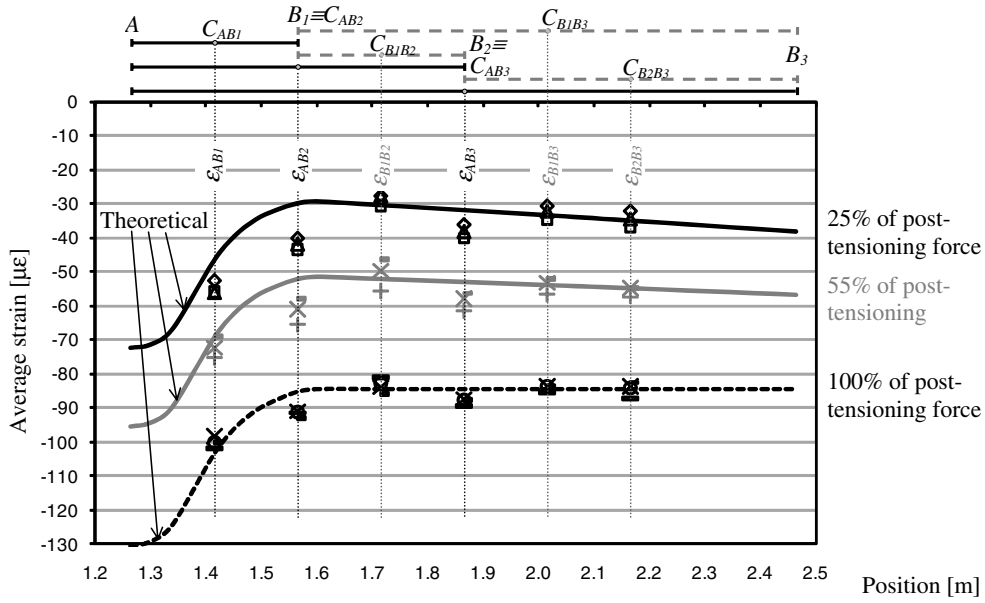

Figure 8. Results of measurements performed by sensors with different gauge lengths.

short-gauge sensors were installed in parallel with long-gauge sensors for direct comparison; (II) the theoretically calculated strain is determined based on linear elastostatics theory, which is not strictly accurate; and (III) small force fluctuations were present at each stage of post-tensioning due to the performance of the post-tensioning device, the friction/sliding of the bridge deck with the formwork, the friction/sliding of tendons within the inner duct, and creep effects in concrete and relaxation effects in tendons. Nevertheless, the analysis presented in this section illustrates well the contents presented in section 3.

All the sensors have the same starting point 'A' and different ending points 'B' (see figure 7), and consequently different centres 'C'. Since the point 'A' of all three sensors is practically in the cross-section where the cross-section changes (see figure 7), a strain field perturbation, i.e. strain concentration, is expected around this point. The strain concentration results from transfer of both axial stresses, mainly introduced by the post-tensioning force, and shear stresses, mainly introduced by reaction from the abutment. The sensors are embedded very close to the centre of gravity of the cross-section, and the theory of elasticity [10] predicts a very small strain perturbation at that location due to the post-tensioning force. The perturbation of the strain field due to shear stresses was assumed to be more important; however, the magnitude and the length of the perturbed zone were expected to be smaller than those induced by concentrated force as presented in subsections 3.3 and 3.5. Since the depth of the cross-section at the location of sensors was slightly shorter than 0.578 m, the perturbed zone was expected to be shorter than 0.289 m. Hence, all three end points 'B' were assumed to be either out of the perturbed zone or just slightly inside this zone. All these assumptions were confirmed by the results.

Besides the direct average strain measurement provided by the three original sensors, three additional strain values can be determined between the extremities of the sensors (between pairs of points 'B') using the following formula:

$$\varepsilon_{C,s_{kj}} = \varepsilon_{B_kB_j} = \frac{\Delta L_{B_jB_k}}{L_{B_jB_k}} = \frac{\varepsilon_{C,s_{jk}} L_{AB_j} - \varepsilon_{C,s_{jk}} L_{AB_k}}{L_{AB_j} - L_{AB_k}} = \frac{\varepsilon_{AB_j} L_{AB_j} - \varepsilon_{AB_k} L_{AB_k}}{L_{AB_j} - L_{AB_k}} (j,k) \in \{(2,1),(3,1),(3,2)\}. \tag{25}$$

Two important properties of the 'measurements' of these three virtual sensors B_1B_2, B_1B_3, and B_2B_3 are as follows: (i) their extremities are in the zone where no perturbation of the strain field is expected, i.e. in the zone where a strain distribution is assumed to follow the elementary theory of beams; (ii) only two values out of three are linearly independent—the third can be represented as a linear combination of two others. The strain measurements obtained by both the original and virtual sensors are compared with the theoretically calculated strain as shown in figure 8.

Before the post-tensioning force was applied, the bridge was supported by the formwork; thus the reactive forces in the abutment and the columns, as well as longitudinal stress and strain components due to dead load were very low, approximately zero. After the first increment of the post-tensioning force was applied, the bridge spans lifted up, the dead load was activated, and reactions arose in the abutment and the columns. Out of the perturbed zone the combination of axial force and bending moments created a parabolic strain distribution but, at the location of sensors, the deviation from the straight line is smaller than the measurement error of the monitoring system (4 $\mu\varepsilon$), and consequently the strain distribution can be considered as linear. The increase in the post-tensioning force causes changes in the strain distribution: the axial strain component (offset) increases by an absolute value while the slope decreases. Perfectly balanced post-tensioning would have as a consequence uniform compression in the beam, with no bending, and the strain distribution would

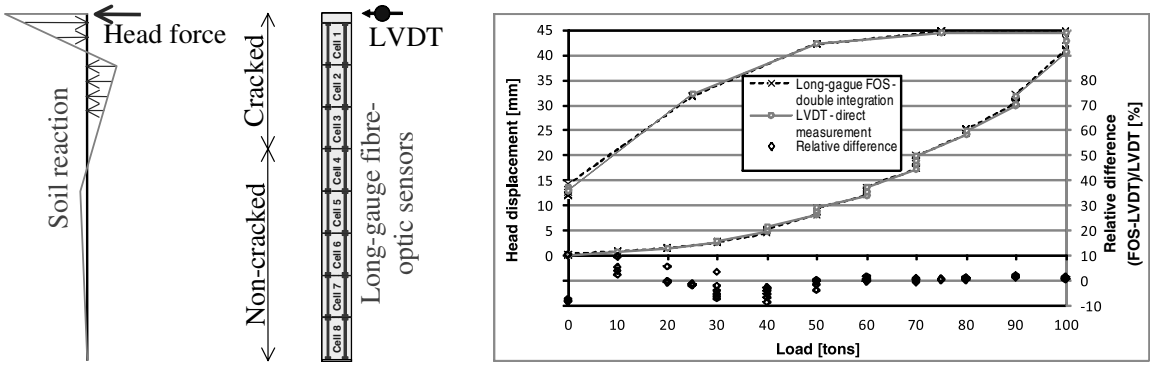

Figure 9. Assumed loading, position of sensors, and displacement of the pile's head.

be constant along the beam. Here it is important to note that an increase in the post-tensioning force will not increase reactions: the dead load and reactions are activated after the first increment of post-tensioning is applied and the spans are lifted up, and an additional increase in the post-tensioning force does not change this equilibrium.

At each stage of post-tensioning, sensor AB_1 measured the highest compression, sensor AB_3 measured the smallest compression, while the measurement of sensor AB_2 was between the measurements of other two sensors. These results were expected since the sensors were installed close to the extremity where the strain field is perturbed by the proximity of the abutment reaction and the change in the cross-section. Based on the linear elastostatics theory, the perturbation of the strain field around point 'A' of the sensors is mainly introduced by shear stresses, which are created by reaction of the abutment, and the magnitude and the length of the zone of the perturbation are practically established after the first step of post-tensioning and kept constant through the other two stages. The sensor measurements confirmed this assumption. Thus, for the original sensors AB_1, AB_2, and AB_3 we can assume that the strain distribution can be expressed as

$$\varepsilon_{C,s} = \varepsilon_{C,s}^{\text{perturbed}} + \varepsilon_{C,s}^{\text{non-perturbed}}, \tag{26}$$

where $\varepsilon_{C,s}^{\text{perturbed}}$ is constant and $\varepsilon_{C,s}^{\text{non-perturbed}}$ is linear. According to the conclusions from subsection 3.2 the error inherent to the gauge length is for a linear distribution equal to zero. Consequently the error inherent to the gauge length is equal only to the error introduced in the zone of perturbed strain. This error is supposed to be constant for each increment of force and is calculated to be -1, -7 and -3 $\mu\varepsilon$ for sensors AB_1, AB_2 and AB_3 respectively (for comparison see half of the diagram shown in figure 5). The ranges of differences between theoretically calculated strains and the measured strains shown in figure 8 are then equal to the sum of the measurement error of the monitoring system (± 4 $\mu\varepsilon$) and the measurement error inherent to the gauge length of the sensors, i.e. -5 to $+3$ $\mu\varepsilon$ for sensor AB_1, -11 to -3 $\mu\varepsilon$ for sensor AB_2, and -7 to $+1$ $\mu\varepsilon$ for sensor AB_3. Among the three original sensors the most accurate was the one with the gauge length approximately equal to half of the depth of the cross-section as suggested in subsection 3.3, and partially in subsection 3.5. However, that was true only because the zone of the strain perturbation was not longer than half of the depth of the cross-section which might not be true in a general case.

Virtual sensors were all mostly out of the perturbed zone, i.e. in the zone with a linear strain distribution; thus their measurement error inherent to the gauge length is equal to zero and the range of differences between theoretically calculated and measured strains is equal to the measurement error of the monitoring system, i.e. -4 to $+4$ $\mu\varepsilon$.

All the ranges of differences for both original and virtual sensors are approximately confirmed in figure 8, i.e. they are in good agreement with the theory developed in previous sections. The aim of this section was to emphasize the differences between measurements obtained using sensors with different gauge lengths installed at approximately the same location, in the zone where the strain field is perturbed. In the next section an application example for a beam-like structure is presented.

5. Application example

The measurement error estimations and consequent recommendations for the selection of the sensor gauge length developed in this paper were proven to be viable through direct and indirect comparisons performed on real structures. The detailed presentation of these comparisons would go beyond the scope of this paper; thus, a summary of one selected project is presented as an illustrative application example. More information on the project presented and other comparisons can be found in the literature [5, 17].

To assess the foundation performance for a new semiconductor production facility in the Tainan Scientific Park, Taiwan, it was decided to perform, among others, a flexure test of pile in a full-scale on-site condition. The pile diameter was 1.20 m and the length was 34.5 m. Horizontal force was applied to the head of the pile and the test was performed in accordance with ASTM D3966-90. The displacement of the head of the pile was directly monitored using a linear variable differential transformer (LVDT) and average strain in the pile was monitored using long-gauge fibre-optic sensors. The sensor position in the pile is given in figure 9.

The reaction of soil was assumed to be piecewise linear distributed as shown in figure 9, which was later confirmed by measurements. Thus, the part of pile consisting of cells

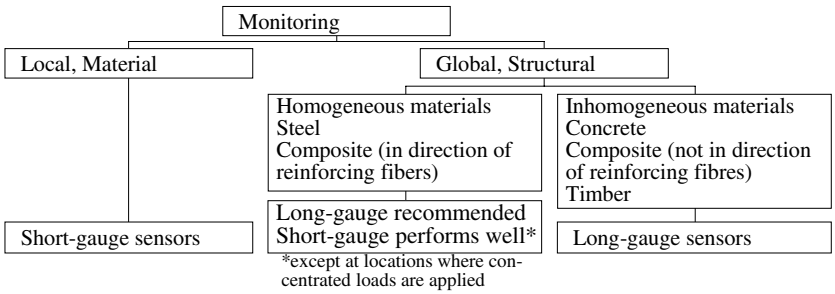

Figure 10. Recommendations for the selection of an appropriate sensor gauge length.

1–3 is expected to crack, while the part of pile consisting of cells 4–8 is not expected to crack (see figure 9). Four-metre long sensors were embedded in concrete during pouring of the pile and the ratio between the sensor gauge length and the length of the pile was 1/8.75. With such a gauge length the relative measurement error at the location of maximum strain in cracked cells 1–3 was expected not to exceed −1% due to the strain distribution (see table 2) and ±10% due to crack openings assuming that the distance between the cracks will not exceed 40 cm (23), and the total relative error was expected to be between −11% and +9% approximately. For the non-cracked part of the pile the relative error was expected not to exceed −1% (see table 2). Each pair of sensors embedded in the same cell allowed for calculus of curvature [5, 14] and double integration of curvature allowed determination of the pile's deformed shape and deflection diagram [5, 14]. Since the error propagates linearly through the process of double integration, it was expected to determine the displacements of pile points with relative error between −11% and +9%.

The displacement of the pile head obtained using double integration of curvature measurement is compared with direct LVDT measurement as shown in figure 9. The comparison confirmed good estimation of relative error and consequently good selection of sensor gauge lengths based on theory recommendations developed in section 3.

6. Conclusions

The conclusions from the above subsections can be in contradiction: for inhomogeneous materials long-gauge sensors are needed, but in the case of a parabolic or broken-line strain distribution, shorter sensors would provide results with lower errors. Consequently, in inhomogeneous materials with a parabolic or broken-line strain distribution it is practically impossible to perform strain monitoring without an error due to the sensors' gauge length. In homogeneous materials, short-gauge sensors can be used, and consequently the error due to sensors' gauge length can be better controlled. However, at locations on the beam where concentrated loads are applied, the short-gauge sensors provide information that is irrelevant to the global monitoring. Thus, the use of long-gauge sensors is recommended in the case of a homogeneous material too, because they overcome the issues related to local perturbations of the strain field, and provide results that reflect global structural behaviour. In addition, they cover larger areas of the structure and therefore, the probability of detecting a critical strain is increased. General principles for the selection of an appropriate sensor gauge length, depending on application type and construction material, are presented in figure 10 (adapted from [5]).

If the qualitative distribution of strain in a monitored structure can be estimated based on numerical models or design assumptions, the errors in the measurements can be evaluated using the principles and expressions presented in this paper. In the case of a beam with a constant cross-section, length L_{beam} and depth h, a preferable gauge length L_s of the sensor can be determined using the following guidelines.

- Monitored cross-section is close to the extremity of the beam: $L_s \geqslant h$ ($L_s \geqslant h/2$ for simple support).
- Monitored cross-section is in the span, close to application point of the concentrated load: $L_s \geqslant h$.
- For inhomogeneous materials $L_s \geqslant 10L_c$ (L_c as defined in figure 6).
- For a beam with a parabolic strain distribution (e.g. due to uniformly distributed load) $L_s \leqslant L_{\text{beam}}/6$.
- For a beam with a broken-line strain distribution (e.g. due to concentrated force) $1.5h \geqslant L_s \geqslant h$ in the general case ($L_s \geqslant h/2$ if two sensors are used), combined if possible with the condition $L_s \leqslant L_{\text{beam}}/10$ (in order to minimize error on strain component generated by M^{BP}).

While designing the sensing network on a structure, the position and the gauge length of the sensors, besides the guidelines presented in this paper, it is important to consider project requirements and overall aims of monitoring.

Acknowledgments

Part of the work was performed at SMARTEC SA, Switzerland. The author would like to thank Mr George Lederman and Mr David Hubbell for help in improving the quality of this paper.

References

[1] Bhatt P, MacGinley T J and Choo B S 2006 *Reinforced Concrete: Design Theory and Examples* 3rd edn (Abingdon: Taylor & Francis) p 767
[2] Measures R 2001 *Structural Monitoring with Fiber Optic Technology* (London: Academic) p 717
[3] Feng X, Sun C, Zhang X and Ansari F 2010 Determination of the coefficient of thermal expansion with embedded long-gauge fiber optic sensors *Meas. Sci. Technol.* **21** 065302

[4] Rodrigues C and Inaudi D 2010 Laboratory and field comparison of long-gauge strain sensing technologies *European Workshop on Structural Health Monitoring (Sorrento, Italy)* paper SS4-05
[5] Glisic B and Inaudi D 2007 *Fibre Optic Methods for Structural Health Monitoring* (Chichester: Wiley) p 262
[6] Hornby I W 1992 The vibrating wire strain gage *Strain Gauge Technology* ed A L Window (Barking: Elsevier) pp 325–46
[7] Chung W, Kim S, Kim N-S and Lee H 2008 Deflection estimation of a full scale prestressed concrete girder using long-gauge fiber optic sensors *Constr. Build. Mater.* **22** 394–401
[8] Glisic B and Inaudi D 2009 Short-gage and long-gage sensors: applicability and interpretation of measurement *Structural Health Monitoring 2009: Proc. 7th Int. Workshop on Structural Health Monitoring (Stanford University, USA, 9–11 September 2009)* ed F-C Chang (Lancaster, PA: DEStech Publications) pp 1659–66
[9] Hibbeler R C 2008 *Structural Analysis* 7th edn (Upper Saddle River, NJ: Prentice-Hall) p 667
[10] Timoshenko S P and Goodier J N 1970 *Theory of Elasticity* (New York: McGraw-Hill) p 567
[11] Ades C S and Lee L H N 1961 Strain-gage measurements in regions of high stress gradient *Exp. Mech.* **1** 199–200
[12] Dotsenko A M and Gorodnichenko V I 1984 Errors of measuring crack length with foil crack gauges and method of taking the errors into account in analysis of the results of cracking resistance tests on materials *Probl. Prochn.* **5** 119–24
Dotsenko A M and Gorodnichenko V I 1984 *Strength Mater.* **16** 757–63 (Engl. Transl.)
[13] Piyasena R 2002 Crack spacing, crack width and tension stiffening effect in reinforced concrete beams and one-way slabs *PhD Thesis* Griffith University, Southport, Queensland, Australia pp 6-1–6-30
[14] Vurpillot S 1999 Analyse automatisée des systèmes de mesure de déformation pour l'auscultation des structures *PhD Thesis* Swiss Federal Institute of Technology—EPFL, Lausanne, Switzerland p 204
[15] Glisic B 2011 Streicker bridge: an on-site SHM laboratory at Princeton University campus *Proc. 1st Middle East Conf. on Smart Monitoring, Assessment and Rehabilitation of Civil Structures (Dubai, UAE)* Paper no 306
[16] Glisic B and Adriaenssens S 2010 Streicker bridge: initial evaluation of life-cycle cost benefits of various structural health monitoring approaches *IABMAS2010—5th Int. Conf. on Bridge Maintenance, Safety and Management (Philadelphia, PA, USA)* Paper no 0396
[17] Glisic B, Inaudi D and Nan C 2002 Piles monitoring during the axial compression, pullout and flexure test using fiber optic sensors *Transp. Res. Rec.* **1808** 11–20